A COMPARISON OF MODAL DECOMPOSITION ALGORITHMS FOR MATCHED-MODE PROCESSING

Nicole Collison and Stan Dosso
School of Earth and Ocean Sciences, University of Victoria, Victoria, BC V8W 3Y2

ABSTRACT

This paper compares a variety of modal decomposition methods used in matched-mode processing (MMP) for ocean acoustic source localization. MMP consists of decomposing far-field acoustic measurements at an array of sensors to obtain the constituent mode excitations (modal decomposition), and then matching these excitations with modelled replica excitations computed for a grid of possible source locations. Modal decomposition can be ill-posed and unstable if the sensor array does not provide an adequate spatial sampling of the acoustic field, so the results of different approaches can vary substantially. Solutions can be characterized by modal resolution and solution covariance; however the ultimate test of the utility of the various methods is how well they perform as part of a MMP source localization algorithm. In this paper, the resolution and variance of the methods are examined using an ideal ocean environment, and MMP results are compared for a series of realistic synthetic test cases, including a variety of noise levels and sensor array configurations. Zeroth order regularized inversion is found to give the best results.

SOMMAIRE

Cet article compare différentes méthodes de décomposition modale utilisées en matched-mode processing (MMP) pour la localisation de source acoustique marine. La méthode MMP consiste à décomposer le champ acoustique mesuré par un réseau de capteurs pour obtenir les excitations modales présentes (décomposition modale), et ensuite à faire correspondre ces excitations avec les excitations calculées par un modèle numérique pour une grille de positions possibles de la source. Le problème de décomposition modale peut être mal posé et instable si les capteurs du réseau ne fournissent pas un échantillonnage spatial adéquate du champ acoustique. Les résultants de differentes approaches peuvent donc varier considérablement. Les solutions peuvent être caractérisées par la résolution modale et la covariance de la solution. Cependant, le critère ultime d'utilité des différentes méthodes est de savoir leur degré de perfomance dans l'algorithme MMP pour la localisation de source. Dans cet article, la résolution et la variance des méthodes sont examinées en utilisant un environnement océanique idéal. Les résultats obtenus avec la méthode MMP sont comparés pour une série de cas réalistique et synthétiques, comprenant différents niveaux de bruit et différentes configurations du réseau de capteurs. Les meilleurs résultats sont obtenus avec la méthode d'inversion basée sur une régularisation d'ordre zéro.

1. INTRODUCTION

Localization of acoustic sources is an important problem in underwater acoustics. Two common approaches to this problem are beamforming (e.g., Burdic[1]) and matched-field processing[2–5] (MFP). Beamforming assumes the incident acoustic fields consist of plane waves, and searches for the inter-sensor time delay and corresponding incidence angle that maximizes the total acoustic power. This provides the bearing of the acoustic source, but not its range and depth. MFP localization matches acoustic pressure fields measured at an array of sensors with replica fields computed for a grid of possible source locations using a numerical propagation model, and can provide localization in range, depth, and bearing. A third method for localizing an acoustic source is matched-mode processing (MMP), which is similar to MFP, but decomposes the measured fields to obtain the excitations of the constituent propagating modes, and matches these with modelled replica excitations.

A potential advantage of MMP over MFP is that subsets of the complete mode set can be considered. Thus,

for example, in cases where bathymetry or geoacoustic parameters of the seabed are poorly known, the matching can be applied only to low-order modes which interact minimally with the bottom.[7,8] However, a potential disadvantage of MMP involves the modal decomposition itself. Modal decomposition represents a linear inverse problem that is non-unique (an infinite number of solutions exist) and can be unstable (small errors on the measured data can lead to large errors on the solution). MMP can provide poor results when the sensor array inadequately samples the acoustic field. If an array contains fewer sensors than there are propagating modes, the highest-order mode functions are under-sampled (spatially aliased), and the inversion is singular. Alternatively, if the array aperture spans too small a fraction of the water column, the lowest-order modes are poorly sampled, leading to an ill-conditioned decomposition problem.

Standard techniques of inverse theory, such as least squares, singular-value decomposition (SVD), and zeroth-order regularization, have been applied to compute a generalized pseudo-inverse for the modal decomposition problem.[9–14] The constructed solution can be characterized in terms of the modal resolution and solution variance. However, for this paper, the ultimate test of a modal decomposition method is how well it performs in source localization, quantified here by the probability of correct localization for realistic synthetic test cases.

This paper compares a variety of modal decomposition techniques by considering solution resolution and variance, and localization performance. Although several papers have compared different approaches to modal decompostion in various ways,[10–13] a truly comprehensive comparison considering resolution, accuracy and localization performance has not been carried out. The paper is organized as follows. Section 2 reviews the underlying theory, including the normal-mode model, pertinent results from linear inverse theory, and an overview of modal decomposition methods. Section 3 provides modal resolution and solution variance comparisons for an ideal ocean environment using a variety of array configurations. In Sec. 4, MMP source localization results for realistic testcases are compared. Finally, Sec. 5 summarizes the paper.

2. THEORY

2.1 Normal Modes

In the far-field, the normal-mode model for the acoustic pressure signal s at depth z due to a point source at a depth z_s and range r can be written as[4,5]

$$s(r,z) = b \sum_{m=1}^{M} \phi_m(z)\phi_m^*(z_s)\frac{e^{ik_m r}}{\sqrt{k_m r}}, \qquad (1)$$

where $*$ denotes complex conjugation, ϕ_m and k_m represent the mth mode function and horizontal wavenumber respectively, M is the total number of propagating modes, and $b = e^{i\pi/4}\sqrt{2\pi}/\rho(z_s)$ where ρ is density. The mode functions are eigenfunction solutions of the depth-separated wave equation, and form an orthonormal set according to[6]

$$\int_0^\infty \frac{\phi_m(z)\phi_n^*(z)}{\rho(z)}dz = \begin{cases} 0 & \text{if } m \neq n, \\ 1 & \text{if } m = n. \end{cases} \qquad (2)$$

The mode function shape depends on $c(z)$ and the boundary conditions applied at the ocean surface and bottom.

In the special case of an ideal ocean consisting of a homogeneous water column ($\rho(z) = \rho$ and $c(z) = c$) of depth h and perfectly-reflecting boundary conditions of a pressure release surface ($s(r,0) = 0$) and a rigid seafloor ($\partial s(r,h)/\partial z = 0$), the mode functions and radial wavenumbers are given by

$$\begin{aligned} \phi_m(z) &= \sqrt{\frac{2\rho}{h}}\sin(\kappa_m z), \\ k_m &= [\omega^2/c^2 - \kappa_m^2]^{1/2}, \end{aligned} \qquad (3)$$

and the vertical wavenumbers κ_m by

$$\kappa_m = \frac{(2m-1)\pi}{2h}. \qquad (4)$$

The horizontal wavenumbers are either real ($\omega^2/c^2 > \kappa_m^2$), corresponding to trapped modes, or purely imaginary ($\omega^2/c^2 < \kappa_m^2$), corresponding to evanescent modes that decay exponentially with range. For a general ocean environment, including variable ocean sound speeds and a layered elastic bottom, simple analytic expressions do not exist for ϕ_m, k_m, and κ_m, but they can be computed numerically using a model such as ORCA.[15]

If the acoustic signal is recorded at a vertical line array (VLA) of N sensors, (1) can be written as a linear matrix equation

$$\mathbf{A}\,\mathbf{x} = \mathbf{s}, \qquad (5)$$

where $\mathbf{s} = [s(z_1), \ldots, s(z_N)]^T$ represents the signal vector and T denotes transpose, $\mathbf{A}$ is an $N \times M$ matrix with columns consisting of the sampled mode functions

$$\mathbf{A} = \begin{bmatrix} \phi_1(z_1) & \ldots & \phi_M(z_1) \\ \vdots & \ddots & \vdots \\ \phi_1(z_N) & \ldots & \phi_M(z_N) \end{bmatrix}, \qquad (6)$$

and $\mathbf{x}$ is a vector of the mode excitations at the receivers

$$\mathbf{x} = b\left[\ \phi_1(z_s)\frac{\exp[ik_1 r]}{\sqrt{k_1 r}}, \ldots, \phi_M(z_s)\frac{\exp[ik_M r]}{\sqrt{k_M r}}\ \right]^T. \qquad (7)$$

Note that $\mathbf{x}$ contains all the information regarding source location (range r and depth z_s). In practical cases, the signal is contaminated by additive noise $\mathbf{n}$, so (5) becomes

$$\mathbf{A}\,\tilde{\mathbf{x}} = \mathbf{s} + \mathbf{n} \equiv \mathbf{p}, \qquad (8)$$

where $\mathbf{p}$ is the vector of measured acoustic pressures $\mathbf{p} = [p(z_1), \ldots, p(z_N)]^T$. Modal decomposition consists of solving (8) for an estimate $\tilde{\mathbf{x}}$ of the true mode excitations $\mathbf{x}$.

2.2 General Linear Inverse Theory

The modal decomposition problem presented in the previous section is representative of a class of discrete linear inverse problems. This and the following section provide an overview of results from linear inverse theory relevant to this paper; more complete treatments are available in Refs. 17–20. If the matrix $\mathbf{A}$ is square and well-conditioned, an exact inverse $\mathbf{A}^{-1}$ and a solution to the inverse problem $\mathbf{x} = \mathbf{A}^{-1}\mathbf{p}$ exist. However, $\mathbf{A}$ is often neither square nor well-conditioned, so methods of linear inverse theory must be employed to obtain a solution. Specific modal decomposition inversion methods for constructing solutions are discussed in Sec. 2.3. This section introduces general methods of examining the characteristics of a solution $\tilde{\mathbf{x}}$ obtained using any generalized inverse $\mathbf{A}^{-g}$ (e.g., Menke[19]),

$$\tilde{\mathbf{x}} = \mathbf{A}^{-g}\,\mathbf{p}. \tag{9}$$

The solution can be characterized by three properties: (i) data misfit, (ii) model resolution, and (iii) solution covariance.

The data misfit (i.e., the level to which the solution fits the data) is typically quantified by

$$\begin{aligned} X^2 &= |\mathbf{G}(\mathbf{A}\,\tilde{\mathbf{x}} - \mathbf{p})|^2 \\ &= \mathbf{p}^\dagger\,(\mathbf{A}\mathbf{A}^{-g} - \mathbf{I})^\dagger\,\mathbf{G}^\dagger\mathbf{G}\,(\mathbf{A}\mathbf{A}^{-g} - \mathbf{I})\,\mathbf{p}, \end{aligned} \tag{10}$$

where $\mathbf{G}$ is a diagonal matrix with the reciprocal of the estimated standard deviation ξ_i for the ith datum p_i on the main diagonal, $\mathbf{I}$ is the identity matrix, and $\dagger$ denotes conjugate (Hermitian) transpose. If the data errors are assumed to be independent, zero-mean, Gaussian-distributed random variables, minimizing (10) leads to the maximum-likelihood solution. Under the assumption of Gaussian noise, the misfit in (10) is distributed according to the central χ^2 distribution.[16] In addition, if the noise terms all have the same standard deviation ξ, (10) simplifies to

$$\chi^2 = \mathbf{p}^\dagger[\mathbf{A}\,\mathbf{A}^{-g} - \mathbf{I}]^2\,\mathbf{p}/\xi^2. \tag{11}$$

If $\mathbf{A}^{-g}$ acts like a right inverse, then $\mathbf{A}\mathbf{A}^{-g} = \mathbf{I}$ and $\chi^2 = 0$. The closer $\mathbf{A}\mathbf{A}^{-g}$ is to $\mathbf{I}$, the smaller the misfit. However, for noisy data, the solution should not be expected to fit the data too closely. For Gaussian noise, a statistically meaningful level for misfit is $\chi^2 = 2N$, the expected value for N complex (noisy) data.[16,20] For the case of correlated noise, (10) can be generalized by replacing the $\mathbf{G}^\dagger\mathbf{G}$ term by the inverse of the estimated data covariance matrix $\langle\mathbf{n}\mathbf{n}^\dagger\rangle$, where $\langle\cdot\rangle$ represents the expected value.

Model resolution indicates how well individual parameters of the model can be resolved. Noting that $\langle\mathbf{p}\rangle = \mathbf{A}\langle\tilde{\mathbf{x}}\rangle$ from (8), it follows that for the noise-free case, $\tilde{\mathbf{x}} = \mathbf{A}^{-g}\,\mathbf{s} = \mathbf{A}^{-g}\,\mathbf{A}\langle\tilde{\mathbf{x}}\rangle$, or

$$\tilde{\mathbf{x}} = \mathbf{R}\langle\tilde{\mathbf{x}}\rangle, \tag{12}$$

where

$$\mathbf{R} = \mathbf{A}^{-g}\mathbf{A} \tag{13}$$

is defined to be the model resolution matrix. If $\mathbf{R} = \mathbf{I}$, each model parameter is perfectly resolved. If $\mathbf{R}$ is diagonally dominant (small non-zero off-diagonal terms), each parameter is well-resolved. However, if $\mathbf{R}$ has significant non-zero off-diagonal terms, the parameters of $\tilde{\mathbf{x}}$ represent weighted averages of the expected parameters, and cannot be individually resolved. Resolution matrices for several different modal decomposition methods and VLA configurations are illustrated in Sec. 3.

The solution covariance is defined as

$$\mathbf{C} = \langle[\tilde{\mathbf{x}} - \langle\tilde{\mathbf{x}}\rangle][\tilde{\mathbf{x}} - \langle\tilde{\mathbf{x}}\rangle]^\dagger\rangle = \mathbf{A}^{-g}\langle\mathbf{n}\mathbf{n}^\dagger\rangle(\mathbf{A}^{-g})^\dagger. \tag{14}$$

For Gaussian errors with the same standard deviation ξ, $\langle\mathbf{n}\mathbf{n}^\dagger\rangle = \xi^2\mathbf{I}$, and

$$\mathbf{C} = \xi^2\,\mathbf{A}^{-g}\,(\mathbf{A}^{-g})^\dagger. \tag{15}$$

The mth diagonal element C_{mm} gives the variance of the mth model parameter $\tilde{x}_m$, with the solution standard deviations given by $\sigma_m = \sqrt{C_{mm}}$. Note that these standard deviations are with respect to the expected solution $\langle\tilde{\mathbf{x}}\rangle$, which only coincides with the true solution for even- and over-determined problems. The off-diagonal terms of $\mathbf{C}$ represent the covariances between solution parameters.

In general, for linear inverse problems, there is a trade-off between solution variance and resolution. The following section illustrates how particular solutions can be developed for the modal decomposition problem by exploiting this trade-off.

2.3 Modal Decomposition Methods

This section briefly reviews the various inversion methods applied to modal decomposition. One of the simplest approaches to modal decomposition is the sampled-mode shapes (SMS) filter. This method is based on the assumption that the modes are orthogonal and applies $\mathbf{A}^\dagger$ as the general inverse to (8) to obtain[9,21]

$$\tilde{\mathbf{x}} \approx \mathbf{A}^\dagger\,\mathbf{p}. \tag{16}$$

Equation (16) provides a fast (no matrix inversion) and effective solution as long as the modes are well-sampled over their entire extent so that the columns of $\mathbf{A}$ are approximately orthonormal. Buck *et al.*[13] noted that the generalized SMS inverse is optimal for detecting a single mode in spatially white noise, but is non-optimal for more than one mode when the spatial modal sampling does not preserve mode orthogonality. They suggest normalizing $\mathbf{A}^\dagger$ by applying a matrix $\mathbf{W}$ so that the diagonal elements of $\mathbf{W}\mathbf{A}^\dagger\mathbf{A}$ are unity, where

$$\mathbf{W} = \mathrm{diag}\left[\|\phi_1(z)\|^{-2}, \ldots, \|\phi_M(z)\|^{-2}\right] \tag{17}$$

and $\|\phi_m\|^2 = \sum_j |\phi_m(z_j)|^2/\rho(z_j)dz$ for j sampled depth points. The modal resolution (13) for the SMS pseudo-inverse is found to be

$$\mathbf{R} = \mathbf{W}\,\mathbf{A}^\dagger\,\mathbf{A}, \tag{18}$$

and the solution covariance (14) is

$$\mathbf{C} = \xi^2\,\mathbf{W}\,\mathbf{A}^\dagger\,\mathbf{A}\,\mathbf{W}^\dagger. \tag{19}$$

This method can perform poorly if an adequate sampling of the modes (to ensure orthogonality) is not possible, particularly in practical cases of an acoustically penetrable seabed where the mode functions extend into the bottom.

The least-squares (maximum likelihood) solution is determined by minimizing the χ^2 misfit

$$\chi^2 = (\mathbf{A}\,\tilde{\mathbf{x}} - \mathbf{p})^\dagger\,\mathbf{G}^\dagger\,\mathbf{G}\,(\mathbf{A}\,\tilde{\mathbf{x}} - \mathbf{p}) \tag{20}$$

by setting $\partial\chi^2/\partial\tilde{\mathbf{x}} = 0$ to yield

$$\tilde{\mathbf{x}} = [\mathbf{A}^\dagger\,\mathbf{G}^\dagger\,\mathbf{G}\,\mathbf{A}]^{-1}\,\mathbf{A}^\dagger\,\mathbf{G}^\dagger\,\mathbf{G}\,\mathbf{p}. \tag{21}$$

Note that if $\mathbf{A}$ is orthogonal and the data have the same uncertainty, the least-squares solution (21) reduces to the SMS solution (16). The least-squares approach provides an unbiased estimate of the true solution (i.e., the solution to the noise-free problem) provided the matrix in square brackets is non-singular. In addition to the possibility of singularity, the matrix can be ill-conditioned, leading to an unstable inversion (i.e., small errors in the data can lead to large errors in the solution).

A common approach for solving ill-conditioned inversions is based on singular-value decomposition (SVD).[16] The SVD of $\mathbf{GA}$ is given by

$$\mathbf{GA} = \mathbf{U}\,\mathbf{\Lambda}\,\mathbf{V}^\dagger, \tag{22}$$

where $\mathbf{U}$ and $\mathbf{V}$ are $N \times M$ and $M \times M$ matrices whose columns are orthonormal eigenvectors, and $\mathbf{\Lambda}$ is a $M \times M$ diagonal matrix of singular values ordered according to decreasing magnitude. Using (22) in (21), the SVD solution to the linear inverse problem is given by

$$\tilde{\mathbf{x}} = \mathbf{V}\,\mathbf{\Lambda}^{-1}\,\mathbf{U}^\dagger\,\mathbf{G}\,\mathbf{p} = \sum_{m=1}^{M} \mathbf{v}_m\,\mathbf{u}_m^\dagger\,\frac{1}{\lambda_m}\,\mathbf{G}\,\mathbf{p}, \tag{23}$$

where the $\mathbf{v}_m$ and $\mathbf{u}_m$ represent the mth columns of $\mathbf{V}$ and $\mathbf{U}$, respectively. Equation (23) is not defined if one or more λ_m are zero, which corresponds to a singular matrix in (21). An ill-conditioned matrix is characterized by one or more λ_m being very small. Equation (23) indicates that small λ_m can cause the errors on the data $\mathbf{p}$ to have a greatly magnified effect on the solution $\tilde{\mathbf{x}}$ (i.e., small λ_m cause instability). Yang[10] and Voronovich *et al.*[11] apply SVD to modal decomposition, but decompose $\mathbf{A}^\dagger\mathbf{G}^\dagger\mathbf{GA}$ instead of $\mathbf{GA}$. However, the SVD of $\mathbf{GA}$ is recommended, because its singular values are the square roots of the singular values of $\mathbf{A}^\dagger\mathbf{G}^\dagger\mathbf{GA}$, which are more numerically stable for small singular values.[16] To stabilize ill-conditioned inversions, the reciprocals of zero or small singular values in (23) can be set to zero, thereby removing their effect on the inversion. If $M - Q$ small singular values are omitted, (23) becomes

$$\tilde{\mathbf{x}} = \sum_{m=1}^{Q} \mathbf{v}_m\,\mathbf{u}_m^\dagger\,\frac{1}{\lambda_m}\,\mathbf{G}\,\mathbf{p}, \qquad Q \le M. \tag{24}$$

How small λ_m needs to be in order to be omitted from the inversion is somewhat arbitrary. Omitting singular values generally decreases the solution variance at the expense of parameter resolution, which can be seen as follows. The solution covariance for (24) is obtained by substituting $\mathbf{A}^{-g} = \sum_{m=1}^{Q} \mathbf{v}_m\mathbf{u}_m^\dagger\mathbf{G}/\lambda_m$ (from 24) into (14), which yields

$$\mathbf{C} = \sum_{m=1}^{Q} \mathbf{v}_m\mathbf{v}_m^\dagger\,\frac{1}{\lambda_m^2}. \tag{25}$$

The $1/\lambda_m^2$ term in (25) is large for small λ_m, so neglecting these λ_m can significantly reduce the solution variance. The resolution matrix (13) for this case is found to be

$$\mathbf{R} = \sum_{m=1}^{Q} \mathbf{v}_m\,\mathbf{v}_m^\dagger. \tag{26}$$

If $Q = M$ in (26), then $\mathbf{R} = \mathbf{I}$ (as $\mathbf{V}$ is orthonormal), indicating unique modal resolution. However, for $Q < M$, columns of $\mathbf{V}$ are omitted, and the resolution is degraded.

The number of singular values removed must be carefully chosen so that resolution is not unduly sacrificed in an effort to reduce variance. In an Arctic application of MMP, Yang[10] noted that the singular values divided naturally into two groups, with the singular values in one group being several orders of magnitude larger than those in the other. He proposed that the large singular values correspond to eigenvectors that span the mode "signal space" while the eigenvectors associated with the small singular values span the mode "noise space," providing a physical basis for neglecting the small singular values. However, when the singular values do not divide naturally into groups, deciding which ones to omit is more difficult. An objective approach is to require that the data be fit to a statistically appropriate level: for example, omit small λ_m until the χ^2 misfit is approximately equal to its expected value. Note that the formulation in (24) applies to both over- and under-determined inversions, although for $Q < M$, the solution is not unbiased: removing singular values stabilizes the inversion by implicitly determining the "smallest" solution in the sense that $|\tilde{\mathbf{x}}|$ is biased to be as close to zero as possible.[16]

A variation of the smallest solution can be formulated using zeroth-order or smallest regularization, which is based on minimizing an objective function Ψ that combines a term representing the data mismatch and a term representing the magnitude of the solution[16]

$$\Psi = |\mathbf{G}(\mathbf{A}\,\tilde{\mathbf{x}} - \mathbf{p})|^2 + \theta\,|\mathbf{H}\,\tilde{\mathbf{x}}|^2. \tag{27}$$

In (27), $\mathbf{H}$ represents an arbitrary weighting, known as the regularization matrix, and θ is a trade-off parameter that controls the relative importance of the two terms in the minimization. Minimizing Ψ with respect to $\tilde{\mathbf{x}}$ leads to

$$\tilde{\mathbf{x}} = [\mathbf{A}^\dagger\,\mathbf{G}^\dagger\,\mathbf{G}\,\mathbf{A} + \theta\,\mathbf{H}^\dagger\,\mathbf{H}]^{-1}\,\mathbf{A}^\dagger\,\mathbf{G}^\dagger\,\mathbf{G}\,\mathbf{p}. \tag{28}$$

For the simple case of an identity weighting in (27), (28) can be expressed as

$$\tilde{\mathbf{x}} = \sum_{m=1}^{M} \mathbf{v}_m\,\mathbf{u}_m^\dagger\,\frac{\lambda_m}{\lambda_m^2 + \theta}\,\mathbf{G}\,\mathbf{p}. \tag{29}$$

From (29), it is apparent that the factor $\lambda_m/(\lambda_m^2+\theta)$ serves as a weighting for the contribution associated with the mth singular value, rather than the factor $1/\lambda_m$ in (23). For an appropriate choice of θ in (28), this weighting is small for small λ_m (rather than large), and a stable inversion is achieved. The trade-off parameter θ in (28) can be set so as to just stabilize the inversion; alternatively, θ can also be set to achieve the expected χ^2 misfit (determining the appropriate trade-off parameter is considered in detail in Collison,[7] and Collison and Dosso[8]). Buck *et al.*[13] and Timonov *et al.*[14] considered smallest regularizations with identity weightings. Voronovich *et al.*[11] considered two forms of (28), one with $\mathbf{H}$=$\mathbf{I}$, and the other with $\mathbf{H} = \text{diag}\,[|\phi_1(z_s)|^{-1},\ldots,|\phi_M(z_s)|^{-1}]$ so as to concentrate the minimization on the mode amplitudes whose excitations at the source are small.

In the case where there are fewer sensors than modes, the modal decomposition is under-determined, with $M-N$ zero singular values indicating spatially aliased modes. For SVD inversion, Yang[10,22] suggested neglecting the aliased high-order modes (effectively set $M=N$) and then inverting the resulting square, non-singular mode matrix. This method only inverts the properly sampled low-order modes. However, omitting the aliased modes from the inversion effectively relegates them to be part of the noise, thereby reducing the signal-to-noise ratio (SNR) by an unknown amount.

3. MODAL RESOLUTION AND VARIANCE IN THE IDEAL OCEAN

The resolution and variance of the modal decomposition results are determined by the VLA configuration and the type of inversion applied. Both of these properties directly affect the success of MMP localization. This section investigates the resolution and variance of various modal decomposition schemes for a simple ocean environment.

The ideal ocean model consists of a uniform water column and boundary conditions of a pressure release surface and a rigid seafloor. Figure 1 illustrates the ideal ocean example used here, consisting of a 300-m water column with a sound speed and density of 1500 m/s and 1.0 g/cm^3, respectively. A 30-Hz source at (r,z) = (6 km, 100 m) in this environment produces 12 propagating modes, shown in Fig. 2. These modes are sine waves confined to the water column (Sec. 2.1), so uniform modal sampling can be explained simply using the sampling theorem of time series analysis (see Ref. 7). Thus, the ideal ocean provides an appropriate starting example to analyze resolution and variance for modal decomposition.

3.1 Under-sampled Case

This section considers the effect of spatial sampling on modal resolution and solution variance. To consider the effects of under-sampling the modes, seven different VLA configurations are considered involving from 12 to 6 sensors; in each case, the sensors are equally spaced over the entire water column. For a 12-sensor VLA, Fig. 3

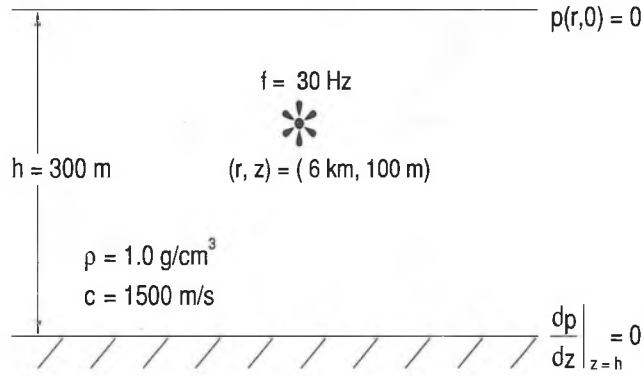

Figure 1: Schematic diagram of the ideal ocean environment.

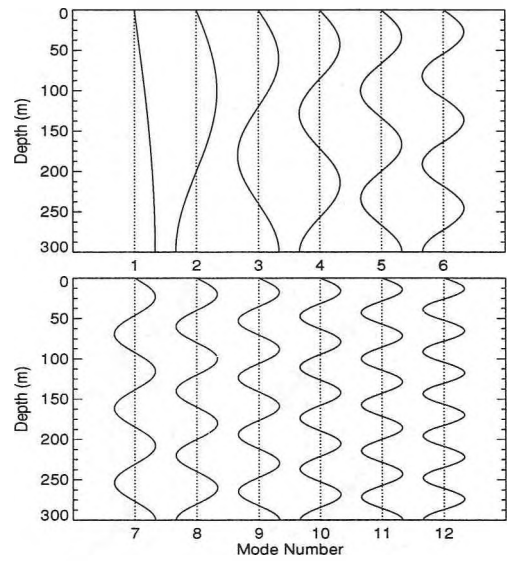

Figure 2: Normal modes for the ideal ocean environment described in Fig. 1.

shows resolution matrices (normalized by their largest values) and corresponding solution standard deviations for various inversion techniques. The SNR of the data in Fig. 3 is taken to be 15 dB, where the (per sensor) SNR is defined

$$\text{SNR} = 10\log\left[|\mathbf{s}|^2/|\mathbf{n}|^2\right]. \qquad (30)$$

From Fig. 3, it is apparent that 12 sensors adequately sample the 12 modes, as indicated by the diagonal resolution matrices. In this figure, the solution standard deviations σ_m are scaled by the true mode excitation values. These (scaled) standard deviations provide a relative measure of the uncertainty of the constructed solution. The SVD inversion in Fig. 3a produces fairly large relative standard deviations. The SMS pseudo-inverse gives only slightly smaller standard deviations, as shown in Fig. 3b. The standard deviations from using smallest regularization (Fig. 3c) are significantly smaller than the other approaches.

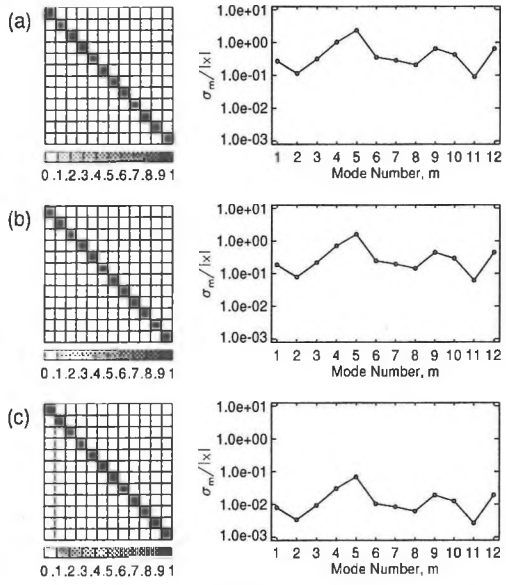

Figure 3: Resolution matrices (normalized by largest values) and corresponding solution standard deviations (normalized by true excitation values) using a 12-sensor VLA spanning the water column for (a) SVD , (b) SMS, and (c) smallest regularization with $\mathbf{H} = \mathbf{I}$.

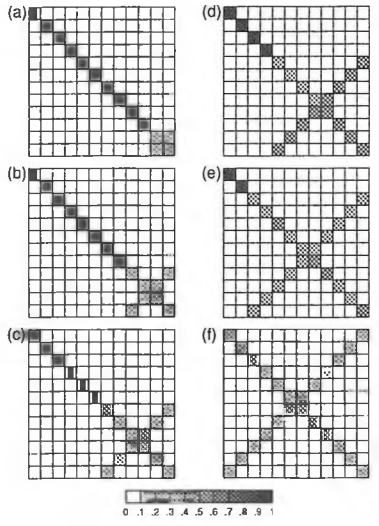

Figure 4: Resolution matrices for 11–6 sensors spanning the water column are given in (a)–(f), respectively. $\mathbf{A}^{-g}$ uses stabilized SVD.

As mentioned previously, spatial aliasing occurs when the modes are insufficiently sampled, resulting in poor resolution. For the ideal ocean, spatial aliasing (and resolution) can be explained by a simple application of the sampling theorem, which states that critical sampling of a sine wave is two points per cycle.[16] In this case, the mode frequency is $f_m = (2m-1)/4h$, according to (4). The spatial power at f_m can contain aliased energy from higher frequencies $f_m + jf_s$ ($j = 1, 2, \ldots$) where $f_s = 1/\Delta z$ is the sampling frequency and Δz is the sampling interval (i.e., the inter-sensor spacing). To avoid aliasing, a mode function must be sampled at least twice per cycle, so the critical (or Nyquist) frequency is $f_c = f_s/2$. Thus, if $f_m \leq f_c$ for all m, the modes are uniquely determined; however, aliasing occurs when $f_m > f_c$. For example, a 12 sensor VLA has $f_s = 12/300$ m^{-1} and $f_c = 24/1200$ m^{-1}, so all of the modes are uniquely sampled as $f_1 < \ldots < f_{12} = 23/1200 < f_c = 24/1200$ m^{-1}; whereas, for a 11-sensor VLA, $f_c = 22/1200$ m^{-1} so the spectral components for f_{12} are aliased. Spectral components at frequencies greater than the Nyquist frequency are aliased with components at lower frequencies for which

$$|f_m| = |f_{m-i} + jf_s|, \tag{31}$$

where $j = \pm 1, \pm 2, \ldots$ and $1 \leq i < m$. Equation (31) determines the lower frequency components with which the higher frequency components are aliased.[7] For instance, returning to the 11-sensor VLA case, the spectral components for f_{12} are aliased with those for f_{11}, determined by evaluating (31) with $j = -1$; this is in complete agreement with the resolution analysis results in Fig. 4a.

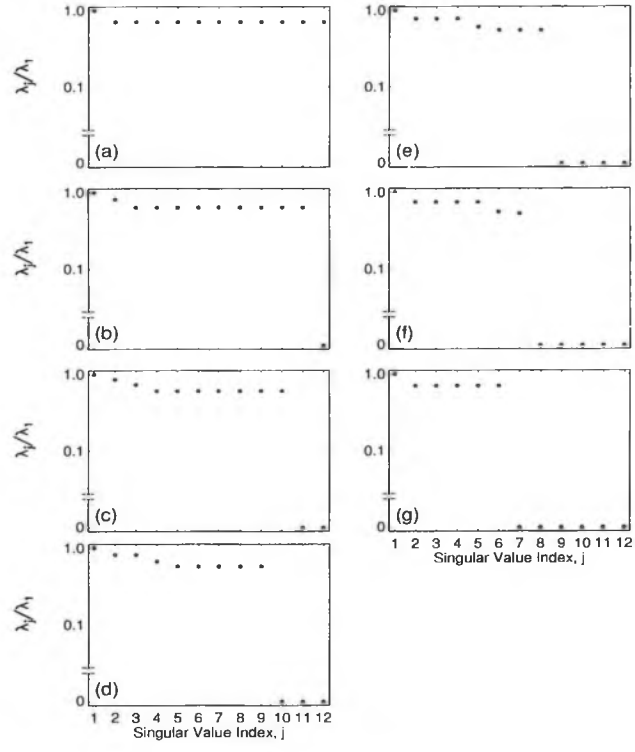

Figure 5: Singular value spectra (normalized by largest value) for 12–6 sensors are shown in (a)–(g), respectively. Note the discontinuity of all vertical axes.

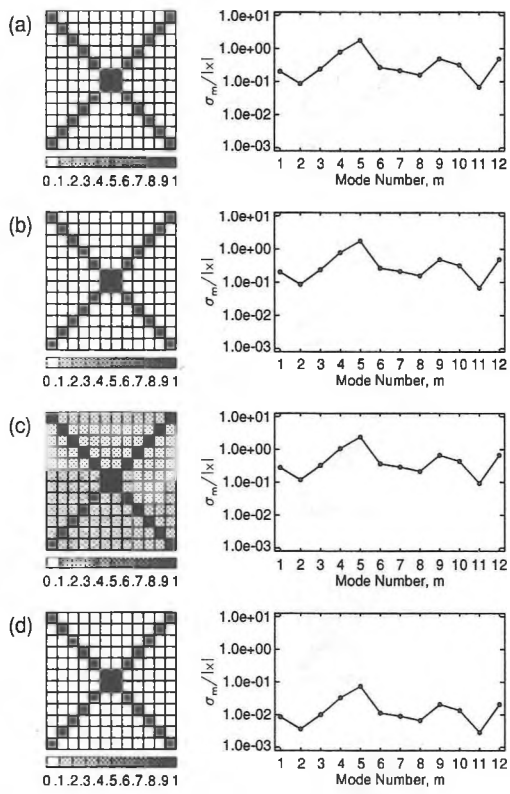

Figure 6: Normalized resolution matrices and solution standard deviations using a 6-sensor VLA for: (a) stabilized SVD, (b) fitted SVD, (c) SMS, and (d) smallest regularization.

The number of high-order modes that are aliased is directly related to the number of zero singular values, as illustrated by comparing Figs. 4 and 5b–g which show the computed resolution matrices and singular value spectra for 11–6 sensors. These figures indicate that as the number of sensors is decreased by one, there is correspondingly one additional zero singular value and one additional aliased pair (linear combination) of modes. In Fig. 4, the higher-order modes are each aliased with only one lower-order mode because the modes are sine functions. For a more general ocean environment and more complicated mode functions, predicting mode aliasing via the sampling theorem is not as simple; however, this information is always provided by modal resolution matrices. Figures 4f and 5g show that for a 6-sensor VLA, there are 6 zero singular values and all modes are affected by aliasing (i.e., the 6 highest-order modes are aliased with the 6 lowest-order ones). This provides an interesting case in which to consider the resolution and standard deviations for various inversion techniques, as shown in Fig. 6. Figure 6a shows the resolution and standard deviations for a stabilized SVD pseudo-inversion omitting the 6 zero singular values. These results are quite similar to the fitted SVD pseudo-inversion, i.e., omitting 7 singular values so $\chi^2 \approx 2N$, as shown in Fig. 6b. Figure 6c and d show the resolution and deviations for SMS pseudo-inversion and smallest regularization, respectively. The standard deviations for smallest regularization are an order of magnitude smaller than those for the other three modal decomposition methods.

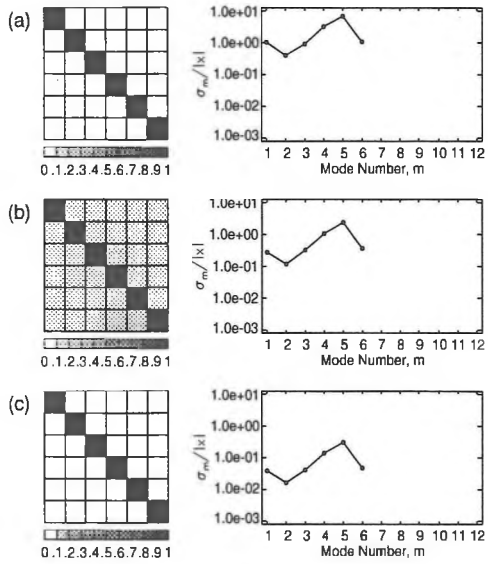

Figure 7: Normalized resolution matrices and solution standard deviations using a 6-sensor VLA for:(a) SVD inversion, (b) SMS, and (c) smallest regularization, all neglecting the aliased high-order modes.

Figure 7 shows inversion results for the same methods when the aliased high-order modes are neglected in the inversion (i.e., delegated to noise), as suggested by Yang.[10,22] Neglecting the aliased high-order modes leads to well resolved low-order modes, but to substantially larger standard deviations for the modes retained than in Fig. 6 (due to the increased noise). Fig. 7c indicates that smallest regularization still provides the smallest standard deviations with respect to the other methods.

3.2 Short-aperture Case

This section considers modal resolution and variance for short-aperture arrays. The VLA configurations considered here all contain 12 sensors and span various fractions of the water column from the entire column (well-sampled) to just the top half. Figure 8 shows the singular value spectra for VLA configurations with apertures of 1.0–0.5 of the water column. The singular values decrease in a continuous manner and do not exhibit the abrupt cut-off evident in the under-sampled case (Fig. 5). In this case, it is not obvious where to truncate the spectrum in an SVD inversion.

One approach is to consider the trade-off between the modal resolution and solution variance. In the case of a well-conditioned $\mathbf{A}$, all the singular values can be included in the inversion, which leads to perfect resolution and small solution standard deviations. For ill-conditioned $\mathbf{A}$, perfect resolution, although possible, occurs at the expense of large solution variance. Figure 9 illustrates the trade-off between resolution and variance for an aperture of 0.5 and SNR=15 dB for various inversion techniques. Figure 9a shows that including all singular values leads to ideal resolution, but that the inversion is unstable with exceedingly large standard deviations. Figure 9b–d shows the trade-off between resolution and solu-

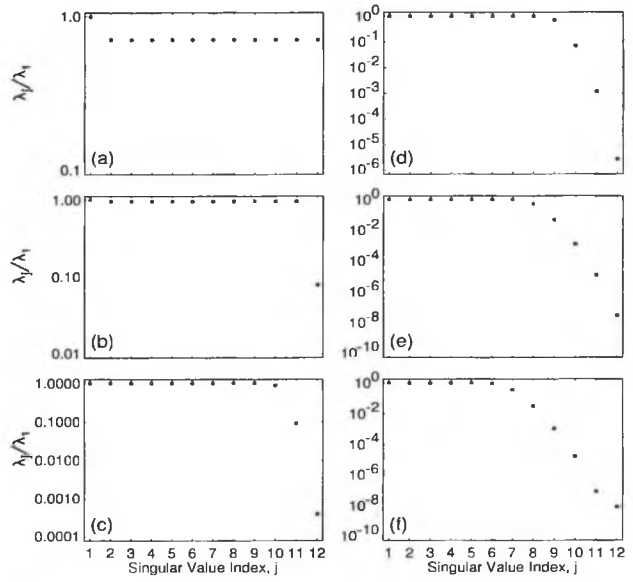

Figure 8: Singular value spectra (normalized by largest value) for apertures of 1.0–0.5 of the water column are shown in (a)–(f), respectively.

tion accuracy for SVD pseudo-inversions. As more singular values are omitted, the resolution of the low-order modes degrades, and the accuracy improves (standard deviations decrease). The fitted SVD pseudo-inversion, shown in Fig. 9e, has significantly smaller standard deviations than the other SVD cases. Figure 9f shows the resolution and accuracy for the SMS pseudo-inversion. For this case, the maximum value of resolution is off the main diagonal (indicating significant modal cross-terms). Figure 9g gives results for smallest regularization. The resolution is similar to that of the fitted SVD pseudo-inversion (Fig. 9e), but the solution standard deviations are substantially smaller.

4. SOURCE LOCALIZATION RESULTS

This section compares various approaches to modal decomposition by considering MMP source localization results for three SNRs, and a variety of VLA configurations. To compare the results of MMP source localization based on various decomposition techniques, it is useful to consider a realistic ocean environment. Source localization techniques are illustrated and compared here for synthetic acoustic data computed for the shallow-water environment illustrated in Fig. 10. The environment consists of a 300-m water column with a typical N.E. Pacific continental shelf sound-speed profile[23] overlying a 50-m thick sediment layer and semi-infinite basement. The sediment layer has a compressional speed of c_p=1650 m/s, shear speed of c_s=300 m/s, density of ρ=1.6 g/cm^3 and compressional and shear attenuations of α=0.3 dB/λ (where λ is the acoustic wavelength). The basement has c_p=2000 m/s, c_s=800 m/s, ρ = 2.1 g/cm^3, and α=0.5 dB/λ. This environment supports 12 propagating modes at a source frequency of 40 Hz, as shown in

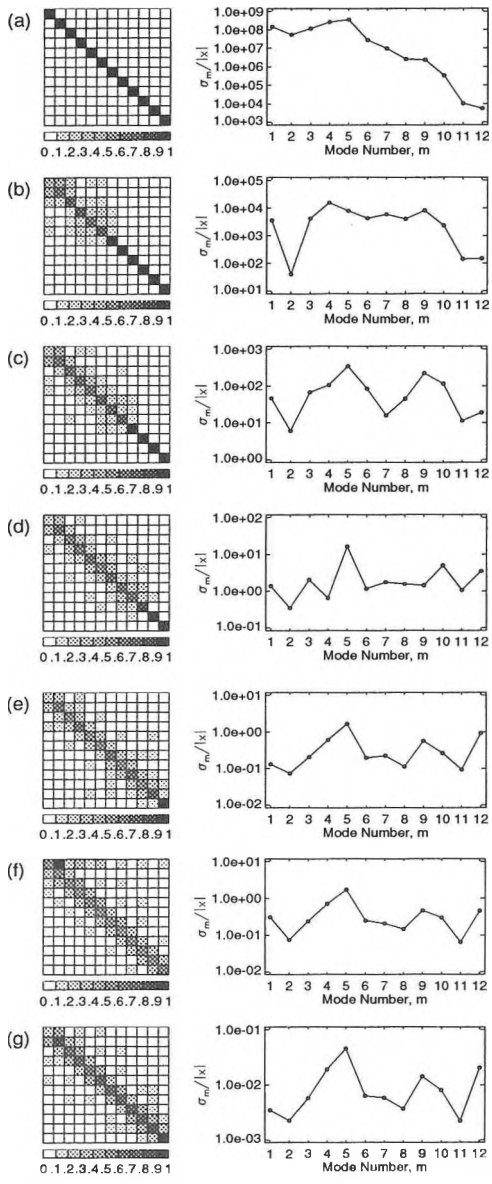

Figure 9: Resolution matrices and solution standard deviations using a 0.5-aperture VLA for (a) SVD (including all λ_j); and SVD omitting λ_j for which (b) $|\lambda_j/\lambda_1| < 10^{-6}$, (c) $|\lambda_j/\lambda_1| < 10^{-4}$, (d) $|\lambda_j/\lambda_1| < 10^{-2}$; (e) fitted SVD; (f) SMS; and (g) smallest regularization.

Fig. 11. In order to compare various approaches to MMP, 100 independent acoustic data sets $\mathbf{p}$ are computed by adding 100 different random realizations of uncorrelated Gaussian noise $\mathbf{n}$ to an acoustic signal $\mathbf{s}$ computed with the wavenumber integration model SAFARI[24] for a source located at (r, z)=(6 km, 100 m). The replica mode excitations used in the matching process are computed using the normal mode model ORCA[15] for all test cases.

Source localization results are considered for three noise levels of SNR = 15, 5, 0 dB, and for a number of VLA configurations that sample the 12 modes in various ways: (i) well-sampled, with 12 sensors equally spaced over

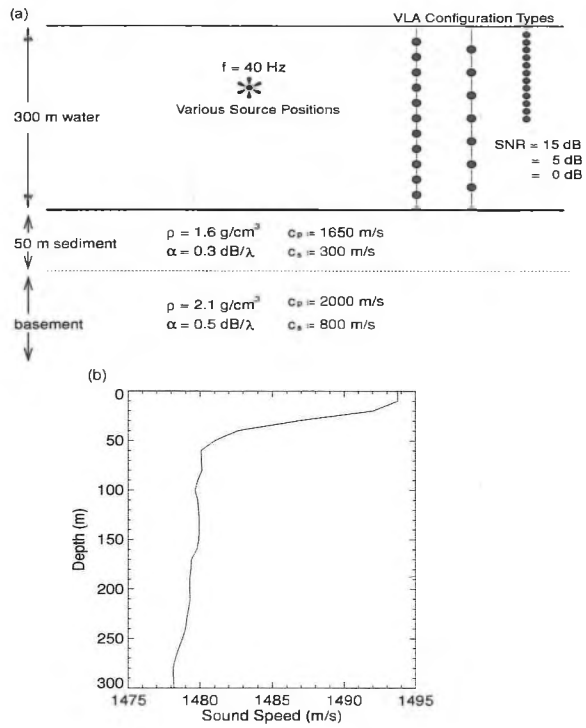

Figure 10: (a) Schematic diagram of the shallow-water environment. Three types of VLA configurations and three SNRs are considered for various source positions. (b) Ocean sound-speed profile.

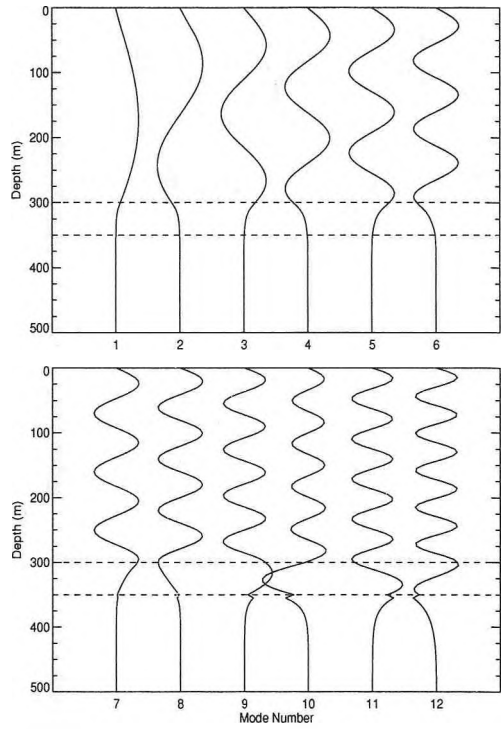

Figure 11: Normal modes produced by a 40-Hz source in the ocean environment described in Fig. 10. Dashed lines denote the water-sediment and sediment-basement interfaces.

the entire water column; (ii) under-sampled, with fewer than 12 sensors equally spaced over the water column; and (iii) short-aperture, with 12 sensors spanning only a fraction of the water column. MMP source localization results are presented for four modal decomposition methods: (i) SMS pseudo-inversion; (ii) stabilized SVD pseudo-inversion omitting singular values λ_j for which $|\lambda_j/\lambda_1| < 10^{-6}$; (iii) fitted SVD pseudo-inversion omitting singular values so $\chi^2 \approx 2N$; and (iv) smallest regularization with $\chi^2 = 2N$. To localize the source, a search grid was adopted that extended from 0–12 km in range with a range increment of 100 m, and 0–300 m in depth with a depth increment of 10 m (i.e., a total of $120 \times 30 = 3600$ grid points). The estimated source location corresponds to the grid point at which the match between the mode excitations was a maximum. The match is quantified using the normalized Bartlett processor

$$B = \frac{|\tilde{\mathbf{x}}^\dagger \mathbf{x}(r,z)|^2}{|\tilde{\mathbf{x}}|^2 \, |\mathbf{x}(r,z)|^2}, \tag{32}$$

where $\tilde{\mathbf{x}}$ represents the constituent mode excitations from the measured fields, and $\mathbf{x}(r,z)$ represents the replica excitations. The correlation at each grid point is indicated on a depth-range plot, known as an ambiguity surface, to obtain a visual representation of the source localization.

Figure 12 shows ambiguity surfaces for the smallest regularization approach to MMP at SNR=5 dB. In this figure, the ambiguity surfaces are plotted in a decibel scale using $-10\log(1-B)$. Figure 12a shows that for a well-sampled case, the source is correctly localized at (r,z)=(6 km, 100 m), with no strong sidelobes. For the under-sampled case, Fig. 12b, the highest peak is located in a sidelobe at (2.5 km, 210 m), resulting in an incorrect localization. For a short-aperture array (Fig. 12c), the source is again incorrectly localized in a sidelobe at (10.4 km, 230 m), and there is no significant peak in the correct source area.

The ambiguity surfaces in Fig. 12 are based on a single set of noisy data. To obtain a more representative comparison of the four approaches to MMP, statistics are compiled for 100 noisy data sets. The relative MMP performance is measured by the estimated probability of correct localization $\hat{P}$, taken to be the fraction of times (for the 100 noisy data sets) that the estimated source location is within a suitably small region about the true source location, defined by ± 200 m in range and ± 10 m in depth.

Figure 13 summarizes the comparative performance of the four approaches to MMP for three SNRs and various VLA configurations. The error bars on each probability measure indicate 90% confidence level for the true probability, computed using[25]

$$\hat{P} \pm 1.645\sqrt{\frac{\hat{P}(1-\hat{P})}{n}}, \tag{33}$$

with $n = 100$ data sets. The first column of Fig. 13 shows localization results for under-sampled cases, and

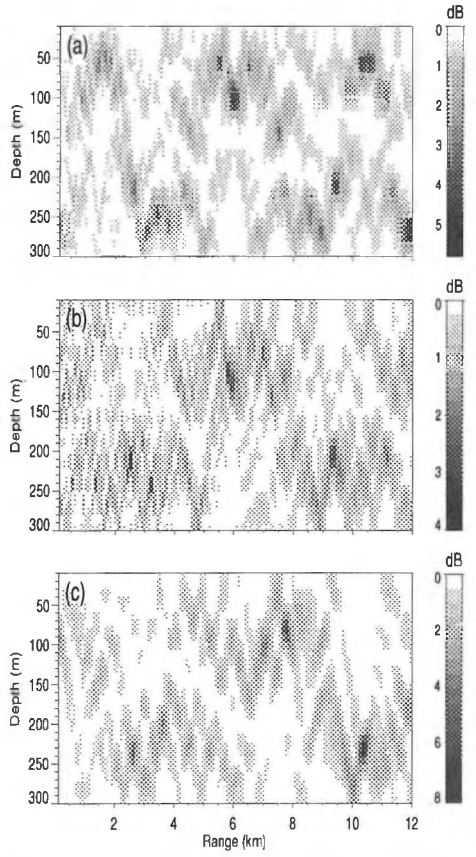

Figure 12: Ambiguity surfaces for (a) well-sampled case, (b) under-sampled case of 6 sensors, and (c) short-aperture case of half the water column, using the smallest regularization approach to MMP at SNR=5 dB.

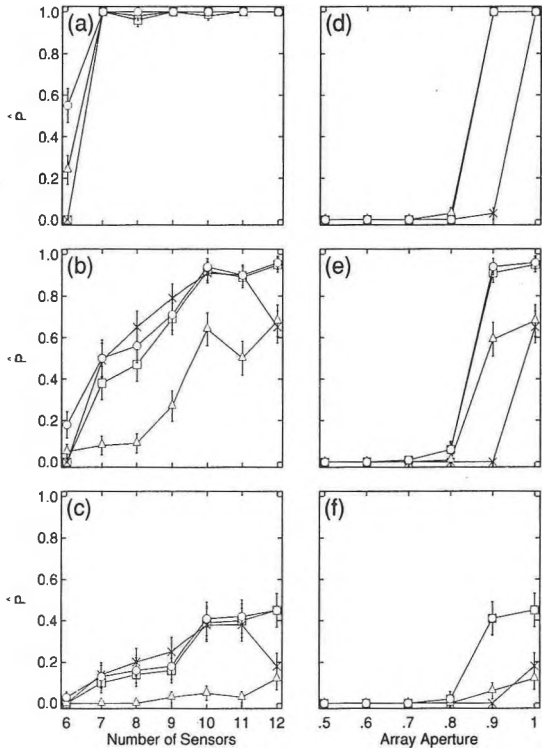

Figure 13: Estimated probability of correct localization $\hat{P}$ for SMS (squares), stabilized SVD (crosses), fitted SVD (triangles), and smallest regularization (circles). Results are given for under-sampled cases and SNRs of (a) 15 dB, (b) 5 dB, and (c) 0 dB. (d)–(f) are the same as (a)–(c), but give results for short-aperture cases. Error bars denote 90% confidence intervals for P.

the second column shows the results for short-aperture cases. In each plot, the well-sampled case (12 sensors, aperture of 1.0) is also included as the right-most point. The rows of the figure correspond to SNRs of 15, 5, and 0 dB (top to bottom).

From Fig. 13, it is apparent that as SNR decreases the localization results for all methods degrade, regardless of the VLA configuration. For a relatively high SNR of 15 dB, Fig. 13a shows that with 7–12 sensors, all the decomposition methods lead to a high probability of source localization. However, with 6 sensors, smallest regularization localizes substantially better than the other three methods (also the case for SNR=5 dB in Fig. 13b). With SNR $\leq$ 5 dB, the under-sampled localization results obtained using smallest regularization and stabilized SVD are quite similar while SMS gives slightly poorer results (Fig. 13b and c). The fitted SVD method has consistently poorer localization results. For array apertures less than or equal to 0.8 of the water column, all methods produce poor localization results, as indicated in Fig. 13d–f. At SNR $\leq$ 5 dB, Fig. 13e and f shows that SMS and smallest regularization have substantially larger probabilities of correct localization than the other two methods for apertures of 0.9 and 1.

As described in Sec. 2.3, Yang[10,22] suggested neglecting the aliased high-order modes for stabilized SVD inversion. To investigate this idea, the aliased modes were neglected in all four modal decomposition methods, with the source localization results given in Fig. 14. Neglecting the aliased high-order modes generally leads to equivalent or better localization results for all methods. The largest improvement in localization results is obtained for SMS. This is likely due to the resulting square mode matrix being closer to orthogonal than the original (singular) rectangular matrix, improving the approximation $\mathbf{A}^{-g} = \mathbf{W}\mathbf{A}^{\dagger}$. Neglecting modes has the added benefit of providing faster inversions, since the dimension of the mode matrix is reduced. From Figs. 13 and 14, it appears that smallest regularization gives slightly better source localization results for more cases than the other methods.

The probabilities of correct localizations shown in Figs. 13 and 14 indicate the relative success of each approach to MMP, but give no indication of the actual distribution of the localization. This can be illustrated by probability ambiguity surfaces (PAS), which show the estimated source positions for the 100 localizations. Figure 15 gives PAS for the well-sampled case with SNR=5 dB. Smallest regularization and SMS (Figs. 15a and b) localize most sources in the correct area, with the incorrect localiza-

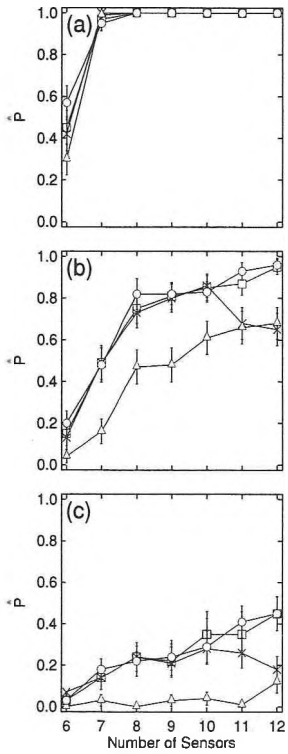

Figure 14: Estimated probability of correct localization $\hat{P}$ for SMS (squares), stabilized SVD (crosses), fitted SVD (triangles), and smallest regularization (circles). Aliased high-order modes are neglected prior to all inversions. Results are given for the under-sampled cases with SNRs of (a) 15 dB, (b) 5 dB, and (c) 0 dB.

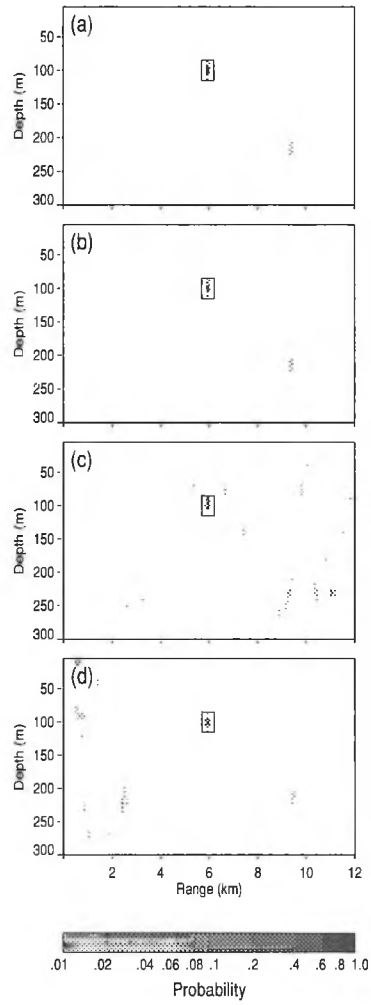

Figure 15: PAS using (a) smallest regularization, (b) SMS, (c) fitted SVD, and (d) stabilized SVD approaches to MMP for the well-sampled case with SNR=5 dB. Gray scale levels indicate the probability of localization for each grid point, and the black boxes indicate the area of correct localization.

tions corresponding to sidelobes of the ambiguity surface (Fig. 12). The SVD methods do not localize as well, as indicated in the increased probabilities of source localization outside of the correct region. The two SVD methods have similar values of $\hat{P}$ for this case, but their PAS indicate that the methods do not always localize at the same position.

Figure 16 shows the PAS for the four approaches to MMP using a 6-sensor VLA at 5 dB, both including and omitting the aliased high-order modes. In Fig. 16a–d, MMP using smallest regularization is the only method that localizes sources in the correct region. It is apparent from the PAS in Fig. 16e–h that neglecting the aliased high-order modes improves all methods to varying degrees. The SMS and stabilized SVD methods are substantially improved, while smallest regularization and fitted SVD are only slightly improved using this array configuration. In this figure, the incorrect localizations again concentrate in areas that correspond to ambiguity-surface sidelobes. Figure 17 shows PAS for a 0.5-aperture VLA with SNR=5 dB. In this figure, smallest regularization, SMS, and fitted SVD approaches to MMP all have high probabilities of localization at an incorrect position corresponding to a sidelobe. Stabilized SVD (Fig. 17d) also localizes incorrectly, but at a different location than the other three methods that does not seem to correspond to a sidelobe from the original ambiguity surface (Fig. 12c).

5. SUMMARY

This paper presents a comprehensive comparison of a variety of approaches to modal decomposition. These comparisons include resolution and variance analyses, and matched-mode processing localization results. The modal methods considered include the sampled mode shape filter, singular value decomposition pseudo-inversion, and smallest regularized inversion. SVD and regularization can be applied to just stabilize the inversion, or to fit noisy (complex) data to the expected value of $\langle \chi^2 \rangle = 2N$ (this can be done exactly for regularization and approximately for SVD). Stabilized and fitted SVD, and fitted regularized inversions were considered here (results for stabilized regularization are similar to those for stabilized

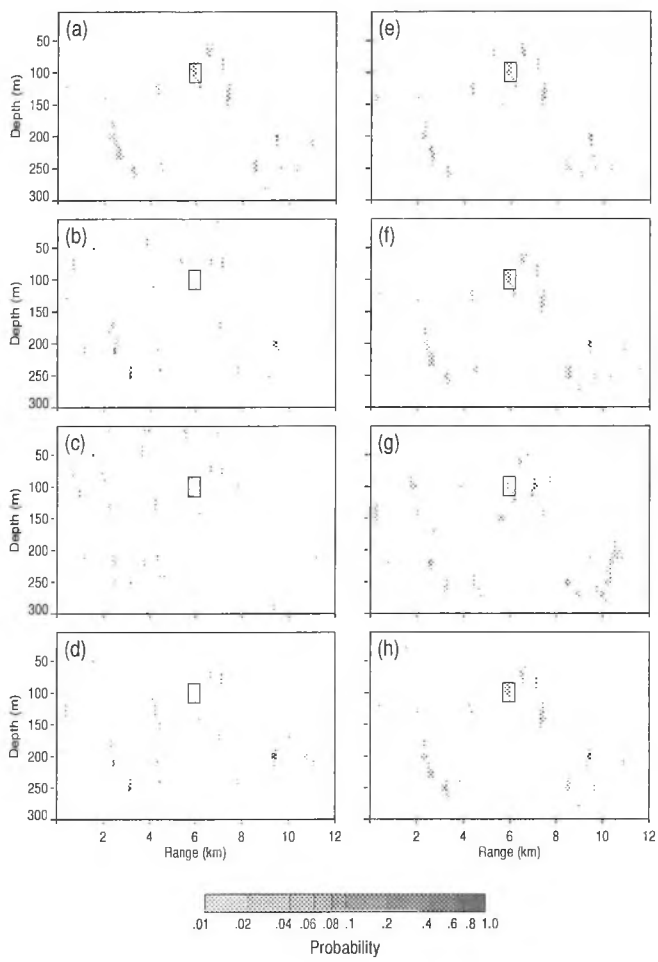

Figure 16: PAS for a 6-sensor VLA using (a) smallest regularization, (b) SMS, (c) fitted SVD, and (d) stabilized SVD with SNR=5 dB. (e)–(h) are the same as (a)–(d), but omit the aliased high-order modes.

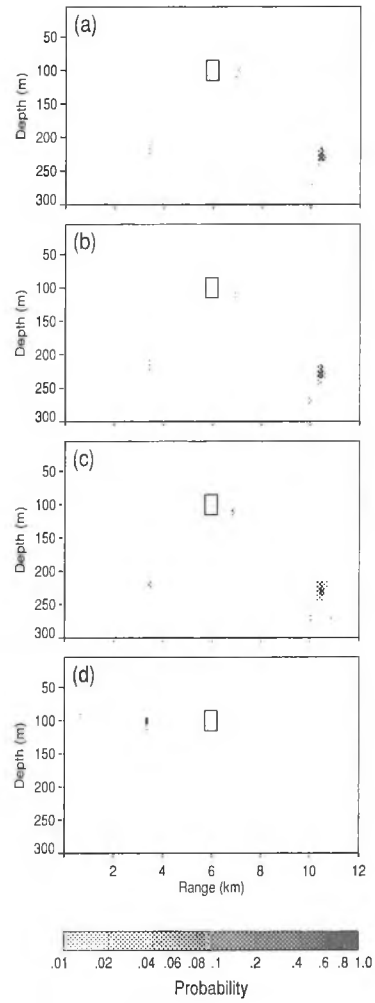

Figure 17: PAS for a 0.5-aperture VLA with SNR=5 dB, using (a) smallest regularization, (b) SMS, (c) fitted SVD, and (d) stabilized SVD.

SVD). These methods were compared for vertical array configurations that properly sampled the acoustic field, and for configurations that under-sampled the field (fewer sensors than modes) or that sampled only a fraction of the water column. High, moderate, and low signal-to-noise ratios were considered. In addition, the idea of omitting aliased high-order modes in under-sampled cases, previously suggested for stabilized SVD inversion, was applied here to all inversion methods.

Modal resolution and variance were examined for the case of a homogeneous ocean with reflecting boundary conditions. In this environment, the modes are sine functions, and hence the resolution analysis can also be explained by simple application of the sampling theorem. For under-sampled cases, the regularized inversion provided the smallest standard deviations. Omitting the aliased high-order modes degraded the accuracy of all methods, but yielded unique resolution of the modes retained. For short-array cases, the singular value spectrum does not exhibit an obvious cut-off, so the number of singular values required to stabilize SVD inversion is somewhat arbitrary, and was shown to control the trade-off between modal resolution and accuracy. Of all the methods, the regularized inversion appeared to provide the best compromise between resolution and accuracy.

The performance of the various modal decomposition algorithms within MMP localization was quantified by the probability of correct localization for a realistic shallow-water environment. For under-sampled cases, it was found that the localization results for regularized, stabilized SVD, and SMS inversions were similar, with fitted SVD performing considerably poorer (as non-zero singular values were omitted in an attempt to approximate $\chi^2 = 2N$). Omitting aliased higher-order modes generally improved the results of all methods, with the regularized inversion giving the best overall results by a small margin. Interestingly, SMS inversion provided the second best results, benefiting the most from omitting aliased modes. Localization results were poor for array apertures of ≤ 0.8 of the water column for this environment. For apertures > 0.8, the regularized and SMS inversions provided the best localization results.

ACKNOWLEDGMENTS

The authors gratefully acknowledge helpful communications with David Thomson, Ross Chapman, Michael Wilmut and Cedric Zala. This work was supported by a National Science and Engineering Research Council (NSERC) research grant.

REFERENCES

[1] W.S. Burdic, *Underwater Acoustic System Analysis 2nd ed.* (Prentice Hall, New Jersey, 1991).

[2] H. P. Bucker, "Use of calculated sound fields and matched field detection to locate sound sources in shallow water," J. Acoust. Soc. Am. **59**, 368–373 (1976).

[3] A. B. Baggeroer, W. A. Kuperman, and P. N. Mikhalevsky, "An overview of matched field methods in ocean acoustics," IEEE J. Oceanic Eng., **18**, 401–424 (1993).

[4] A. Tolstoy, *Matched-field Processing for Underwater Acoustics.* (World Scientific, Singapore, 1993).

[5] F.B. Jensen, W. A. Kuperman, M.B. Porter, and H. Schmidt, *Computational Ocean Acoustics.* (AIP Press, New York, 1994).

[6] G.V. Frisk, *Ocean and Seabed Acoustics.* (Prentice-Hall, New Jersey, 1994).

[7] N.E. Collison, "Regularized matched-mode processing for ocean acoustic source localization," M.Sc. thesis, University of Victoria, Victoria, Canada, 1999.

[8] N.E. Collison and S.E. Dosso, "Regularized matched-mode processing for source localization," J. Acoust. Soc. Am. **107**, 3089–3100 (2000).

[9] C.T. Tindle, K.M. Guthrie, G.E. Bold, M.D. Johns, D. Jones, K.O. Dixen, and T.G. Birdsall, "Measurements of the frequency dependence of normal modes," J. Acoust. Soc. Am. **64**, 1178–1185 (1978).

[10] T.C. Yang, "A method of range and depth estimation by modal decomposition," J. Acoust. Soc. Am. **82**, 1736–1745 (1987).

[11] A. G. Voronovich, V. V. Goncharov, A. Yu. Nikol'tsev, and Yu. A. Chepurin, "Comparative analysis of methods for the normal mode decomposition of a sound field in a waveguide," Sov. Phys. Acoust. **38**, 365–370 (1992).

[12] K.V. Horoshenkov and J.W.R. Griffiths, "On using normal mode decomposition as an approach to the acoustic tomography problem," Acustica **80**, 260–267 (1994).

[13] J.R. Buck, J.C. Preisig, and K.E. Wage, "A unified framework for mode filtering and the maximum a posteriori mode filter," J. Acoust. Soc. Am. **103**, 1813–1824 (1998).

[14] A. Timonov, "Development of a spectral regularization modal decomposition algorithm," *EDRD/DREA Contractors Report 9601*, Defence Research Establishment Pacific, Victoria BC, Canada (1996).

[15] E.K. Westwood, C.T. Tindle, and N.R. Chapman, "A normal mode model for acousto-elastic ocean environments," J. Acoust. Soc. Am. **100**, 3631–3645 (1996).

[16] W. H. Press, B. P. Flannery, S. A. Teukolsky, and W. T. Vetterling *Numerical Recipes - The Art of Scientific Computing 2nd ed.* (Cambridge U. P., Cambridge, 1992).

[17] L. R. Lines and S. Treitel, "Tutorial: A review of least-squares inversion and its application to geophysical inverse problems," Geophys. Prosp. **32**, 159–186 (1984).

[18] C. van Schooneveld, "Inverse problems: A tutorial survey," in *Underwater Acoustic Data Processing*, edited by Y. T. Chan, (Kluwer, The Netherlands, 1989) pp. 393-411.

[19] W. Menke, *Geophysical Data Analysis: Discrete Inverse Theory.* (Academic Press, New York, 1984).

[20] J.A. Scales, P. Docherty, and A. Gersztenkorn, "Regularisation of nonlinear inverse problems: Imaging the near-surface weathering layer," Inverse Problems **6**, 115–131 (1990).

[21] R. H. Ferris, "Comparison of measured and calculated normal-mode amplitude functions for acoustic waves in shallow water," J. Acoust. Soc. Am. **52**, 981–988 (1972).

[22] T.C. Yang, "Effectiveness of mode filtering: A comparison of matched-field and matched-mode processing," J. Acoust. Soc. Am. **87**, 2072–2084 (1990).

[23] M. L. Taillefer, "Range dependent matched-field source localization and tracking in shallow water in a continental slope region of the North-east Pacific Ocean, " M.Sc. thesis, University of Victoria, Victoria, Canada, 1998.

[24] H. Schmidt, "SAFARI: Seismo-acoustic fast field algorithm for range-dependent environments," *SACLANT ASW Research Centre Rep. SR-113*, La Spezia, Italy (1988).

[25] J.L. Devore, *Probability and Statistics for Engineering and the Sciences 3rd ed.* (Brooks Cole Pub., Pacific Grove CA, 1991).

Gunnar Rasmussen Acoustic Solutions:

Precision Acoustic Measurement Instrumentation

Condenser Microphones and Preamplifiers
Intensity Probes
Outdoor Microphones / Hydrophones
Calibration Instrumentation and Accessories

G.R.A.S.
Sound & Vibration

Represented in Canada by

NOVEL DYNAMICS INC.
Dynamic Test and Analysis Systems

Integrated Solutions from World Leaders

Novel Dynamics Inc.
Phone 519-853-4495 Fax 519-853-3366
Email: metelka@aztec-net.com
Ottawa Office 613-599-6275 Fax 613-599-6274